

Estimating the Impacts and Uncertainty of Climate Change on the Hydrology and Water Resources of the Koshi River Basin

Anshul Agarwal, Mukand S. Babel and Shreedhar Maskey

Abstract In this study, projections of temperature and precipitation in future periods and their impacts on hydrology and water resources of the Koshi River Basin in Nepal were investigated. The statistical downscaling model Long Ashton Research Station Weather Generator (LARS-WG) was used to downscale low-resolution data from ten general circulation models (GCMs) and three IPCC SRES scenarios (B1, A1B, and A2). The physically based hydrological model Soil and Water Assessment Tool (SWAT) was used to analyse the impacts of climate change on hydrology. LARS-WG simulated the baseline period (1981–2000) climate quite satisfactorily. Changes in climate and hydrological variables are presented at monthly and annual scales for three future periods: 2011–2030, 2046–2065, and 2080–2099. The results indicate that the Koshi basin tends to become warmer in the future as projected by all GCMs under three SRES scenarios. Changes in precipitation and streamflow are not univocal and vary depending on the GCM, GHGES. The difference in the projection of flow varies by as much as –35 to 51 % under the A1B scenario during the 2055s. The maximum increase in flow is projected during spring season with increase of 23 and 25 % during the 2055s and 2090s, respectively, under the A1B scenario. Similarly, the range of projections for all water balance components is very large. The water balance components: surface flow, baseflow, and water yield may decrease or increase in future periods, as GCMs do not agree on the direction of change. The potential ET and actual ET are projected to increase as projections from all GCMs and scenarios indicate, although a great deal of uncertainty exists in the magnitude of change.

A. Agarwal (✉)

Regional Integrated Multi-Hazard Early Warning System, PO Box 4,
Klong Luang, Pathum Thani 12120, Thailand
e-mail: anshul.agarwal@ait.asia

A. Agarwal · M.S. Babel

Asian Institute of Technology, PO Box 4, Klong Luang, Pathum Thani 12120, Thailand
e-mail: msbabel@ait.asia

S. Maskey

UNESCO-IHE Institute for Water Education, PO Box 3015, 2601,
DA Delft, The Netherlands
e-mail: s.maskey@unesco-ihe.org

The potential ET is projected to increase in the range of 6–24 % in the 2090s. There is high variability among the models and scenarios for projections, and the variability increases with future time periods.

Keywords Climate change · GCM · GHGES · LARS-WG · SWAT · Uncertainty

1 Introduction

The global climate projections in the Fourth Assessment Report of IPCC 2007 concluded that global mean atmospheric temperature is likely to increase between 1.8 and 4.0 °C by the end of this century. This projected change in temperature is likely to intensify the hydrological cycle and average mean water vapour, and precipitation is likely to increase. As a result, hydrological systems are anticipated to experience, not only changes in the average availability of water, but also changes in extremes (Zhang et al. 2011). Mountains being repositories of biodiversity, water and other ecosystem services are among the most fragile environments. The various global changes are creating enormous pressures on the mountains (Sharma et al. 2007). The assessment of future climate is based on different greenhouse gas (GHG) emission scenarios which are the product of very complex dynamic systems, determined by driving forces such as demographic growth, socio-economic development, and technological change (Anandhi et al. 2008). Global climate models (GCMs) are used to estimate the consequences of these developments on the climate in future periods. The outputs of GCMs are usually available at resolutions of 100's of km, and thus, they do not resolve sub-grid scale features and topographic effects that are of significance to many impact studies (Moriondo and Bindi 2006). Future climate projections on a much finer scale are required for impact studies at regional scales (Tisseuil et al. 2010).

To bridge the gap between scales of climate information provided by GCMs and those required for impact studies at regional or local scales, downscaling is used. Basically, two fundamental approaches exist for downscaling: dynamical downscaling (DD) and statistical downscaling (SD). In the dynamical approach, a higher resolution climate model (RCM) is embedded within a GCM. In the statistical approach, various statistical methods are used to establish empirical relationships between GCM output, climate variables, and local climate (Maraun et al. 2010). SD methods are easier and more readily applied to develop higher resolution climate scenarios for impact studies and thus more widely adopted (Chiew et al. 2010). The SD techniques can be grouped into three categories: weather typing method, stochastic weather generators, and regression methods.

The Long Ashton Research Station Weather Generator (LARS-WG) is a stochastic weather generator developed by Semenov and Barrow (1997) for statistical downscaling. Several studies (such as Hashmi et al. 2011) have compared the performance of LARS-WG with other statistical downscaling techniques and have

concluded that LARS-WG can be adopted with confidence for climate change studies. LARS-WG has been applied in climate change impact studies in many research studies, such as in the Saguenay watershed in northern Quebec, Canada (Dibike and Coulibaly 2005); in Montreal, Canada (Nguyen 2005) and in different locations in Europe (Semenov and Stratonovitch 2010). The description of the latest version of LARS-WG, called LARS-WG 5 and its capabilities, is given in Semenov and Stratonovitch (2010). LARS-WG 5 incorporates climate projections from 15 GCMs used in the IPCC-AR4.

A large number of uncertainties exist at the various stages of future climate projections and hydrological analysis, which impose a challenge for impact analysis studies. Uncertainty in climate projections comes mainly from GCMs, SRES scenarios, downscaling methods, and the internal variability of climates (Hawkins and Sutton 2010). The models used for impact analysis (e.g. hydrological models) also bring uncertainty to the assessment of the impacts of climate change (Bastola et al. 2011; Minville et al. 2008). An estimate of the uncertainty in climate projections is potentially valuable for policy makers and planners (Stott and Kettleborough 2002).

This study was conducted in the Koshi River Basin. The Koshi flows through China, Nepal, and India and is one of the largest tributaries of the Ganges. The Koshi River Basin consists of seven major sub-basins (Sun Koshi, Indrawati, Dudh Koshi, Tama Koshi, Bhote Koshi, Arun, and Tamor) all originating from the Himalayas. The Sun Koshi joins the Indrawati and then moves on south-eastwards to collect the following rivers: Tama Koshi, Bhote Koshi, Dudh Koshi and join with Arun and Tamor at Tribeni. About 82 % of the Arun catchment lies in the Tibet Autonomous Region of China. The Sun Koshi and Tama Koshi also have remarkably large catchment areas in the Tibet Autonomous Region of China (WWF 2009). The Koshi basin, characterised as highly varied in climate and geographical features, spans latitudes between 26° 51'N and 29° 79'N and longitudes between 85° 24'E and 88° 57'E. The elevation of the basin ranges from about 65 m in the Terai to over 8,000 m in the high Himalayas (Fig. 1). A large part of the Koshi basin (almost 65 %) is above 4,000 m in elevation.

Many studies confirm that major parts of the Koshi and other river basins in Nepal are undergoing warming trends as well as changes in the precipitation pattern (Agrawala et al. 2003; Bartlett et al. 2010; Chhetri 2010; Shrestha and Devkota 2010). Despite progress in understanding the impact of climate change on water resources, there has been a lack of research in investigating the element of uncertainty. To address the issue, this study analysed future climates using projections from multi-models and multi-scenarios. Projections from different GCMs for various scenarios were then used to investigate the climate change impacts on water resources. This analysis will help in managing water more efficiently and making the necessary plans for adaptation to changing climatic conditions in the Koshi basin.

In this study, the climate projections for the Koshi River Basin were investigated using data from multiple GCMs for three emission scenarios. The impact of climate change on the hydrology of the Koshi basin was analysed using the Soil and Water Assessment Tool (SWAT) model. The uncertainty of GCMs and SRES scenarios in

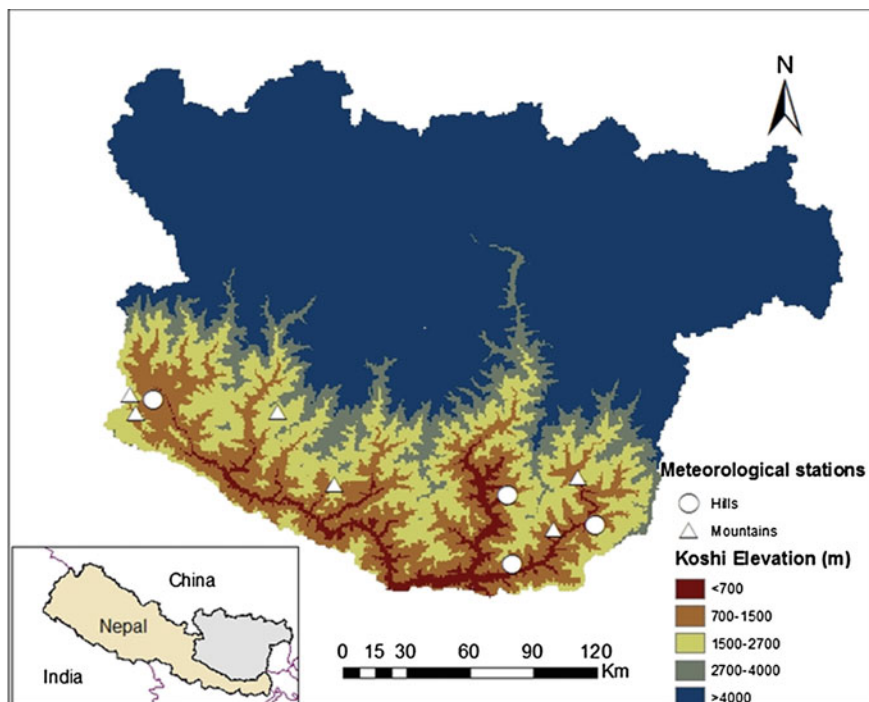


Fig. 1 Elevation range and meteorological stations in the Koshi basin

future climate projections and the hydrology of the Koshi basin were then estimated. The uncertainty resulting from downscaling methods and hydrological model parameters were not analysed in this study.

2 Materials and Methods

The observed daily climate data for the period 1971–2008 were obtained from the Department of Hydrology and Meteorology (DHM), Nepal. The future climate data were downloaded from the IPCC-data distribution centre website.¹ Data from ten GCMs included in IPCC AR4 were considered in this study. The data for these GCMs for selected SRES scenarios are available through LARS-WG5. The GCMs used in the study are listed in Table 1.

Three emission scenarios (B1, A1B, and A2), which represent low, medium, and high emissions of GHG with respect to the prescribed concentrations relative to SRES, were considered in this study. A stochastic weather generator LARS-WG

¹ <http://www.ipcc-data.org/>.

Table 1 Global climate models used in the study

No.	Model	Research centre	Resolution		Scenarios	Vintage
			Atmospheric	Ocean		
1	ECHAM 5	MPI, Germany	$1.87^0 \times 1.87^0$	$1.5^0 \times 1.5^0$	B1, A1B, A2	2005
2	MRI-CGCM2.3	MRI, Japan	$2.8^0 \times 2.8^0$	$2.5^0 \times 2.0^0$	B1, A1B	2003
3	HadCM3	Hadley Centre UK	$2.5^0 \times 3.75^0$	$1.25^0 \times 1.25^0$	B1, A1B, A2	2000
4	CGCM 3.1	CCCMA Canada	$2.8^0 \times 2.8^0$	$1.4^0 \times 1.0^0$	A1B	2005
5	MK3	CSIRO, Australia	$1.9^0 \times 1.9^0$	$1.9^0 \times 1.9^0$	B1, A1B	2001
6	CNCM3	CNRM, France	$1.9^0 \times 1.9^0$	$2.0^0 \times 2.0^0$	A1B, A2	2004
7	IPCM4	IPSL, France	$2.5^0 \times 3.75^0$	$2.0^0 \times 2.0^0$	B1, A1B, A2	2005
8	GFCM21	GFDL, USA	$2.0^0 \times 2.5^0$	$1.0^0 \times 1.0^0$	B1, A1B, A2	2005
9	CCSM3	NCAR, USA	$1.4^0 \times 1.4^0$	$1.0^0 \times 1.0^0$	B1, A1B, A2	2005
10	INCM3	INM, Russia	$4.0^0 \times 5.0^0$	$2.5^0 \times 2.0^0$	B1, A1B, A2	2004

(Semenov and Barrow 1997) was used in this study. A description of the latest version of model LARS-WG 5 and its capabilities is given in, Semenov and Stratonovitch (2010). The model was downloaded from Rothamsted Research.² LARS-WG can generate synthetic daily datasets of precipitation, minimum and maximum temperature, and solar radiation based on observed weather, and generally 20 or 30 years of daily climate data are used in order to capture real climate variability and seasonality. Based on the relative monthly changes in mean daily precipitation, wet and dry series duration, temperature and temperature variability between current and future periods predicted by the GCM, and local station climate variables are adjusted proportionately to represent climate change.

The data required to develop the SWAT model for the Koshi basin were compiled using global data sources. A Digital Elevation Model (DEM) of 90 m resolution was obtained from the Shuttle Radar Topography Mission (SRTM). The soil map used was from the Soil Terrain Database (SOTER), which shows that the Koshi basin has 11 soil types, with Gleyic Leptosols (soil texture clay loam) and Gleyic Phaeozems (soil texture sand) as the dominant soil types. Land cover data were obtained from MODIS land cover type products MCD12Q1 available at the spatial resolution of 500 m for the period 2001–2010. The weather data used for developing the SWAT model is: daily precipitation, minimum and maximum temperature, relative humidity, solar radiation, and wind speed. A large part of the Koshi basin lies in an elevation above 3,000 m where observation stations are not available. To overcome this deficit, a temperature lapse rate of -5.7 °C/km was

² <http://www.rothamsted.ac.uk/mas-models/larswg/download.php>.

incorporated and precipitation data was used from Asian Precipitation Highly Resolved Observational Data Integration Towards Evaluation of Water Resources (APHRODITE) which contains gridded data and is available at a spatial resolution of 25 km.

The SWAT model was developed for the Koshi basin using the data mentioned above. The model performance to simulate the flow was evaluated for the Koshi River and three major tributaries, Sun koshi, Arun, and Tamur. The hydrological data from the DHM, Nepal was available for the years from 1990 onwards. Data for the period 1990–2000 were considered for model calibration and 2001–2008 were considered for model validation. Three statistical parameters: coefficient of determination (R^2), percentage volume error (VE), and Nash–Sutcliffe efficiency (NSE) were used in this study to analyse model performance during calibration and validation.

The calibrated and validated SWAT model was used to analyse the impacts of future climate change on hydrology and water resources in the Koshi basin. The minimum and maximum temperature and precipitation was downscaled using LARS-WG for 10 temperature and 60 precipitation stations located in the Koshi basin were used to evaluate the hydrological parameters and water balance components in the future periods. The solar radiation and relative humidity for the future periods were simulated in SWAT using the WXGEN weather generator. WXGEN uses rainfall and temperature data from each scenario based on the assumption that the occurrence of rain on a given day has a major impact on the relative humidity and solar radiation on that day (Ficklin et al. 2009). The analysis in this study focuses on three periods over the twenty-first century; an early-century period 2011–2030 (2020s), a mid-century period 2046–2065 (2055s), and a late-century period 2080–2099 (2090s). The period 1981–2000 is considered as the baseline period.

3 Results and Discussion

3.1 Model Calibration and Validation

3.1.1 LARS-WG

The performance of the LARS-WG model was tested against the historical data (daily T_{\min} and T_{\max}) for the baseline period (1971–2000). The mean monthly bias values for T_{\min} , T_{\max} , and precipitation for ten meteorological stations located in the Koshi basin (Fig. 1) are presented in Fig. 2. The LARS-WG performance was evaluated for all 60 precipitation stations used in this study although results are presented here for only ten stations. The bias values for T_{\min} and T_{\max} were mostly close to zero, with a narrow range of ± 0.5 °C. The mean monthly bias for precipitation was also found to be satisfactory for all the stations. The higher bias values were obtained during the months of the monsoon season (JJAS) compared to the remaining months. The mean annual bias was close to zero, which may be because of the positive bias in certain months being balanced out by the negative

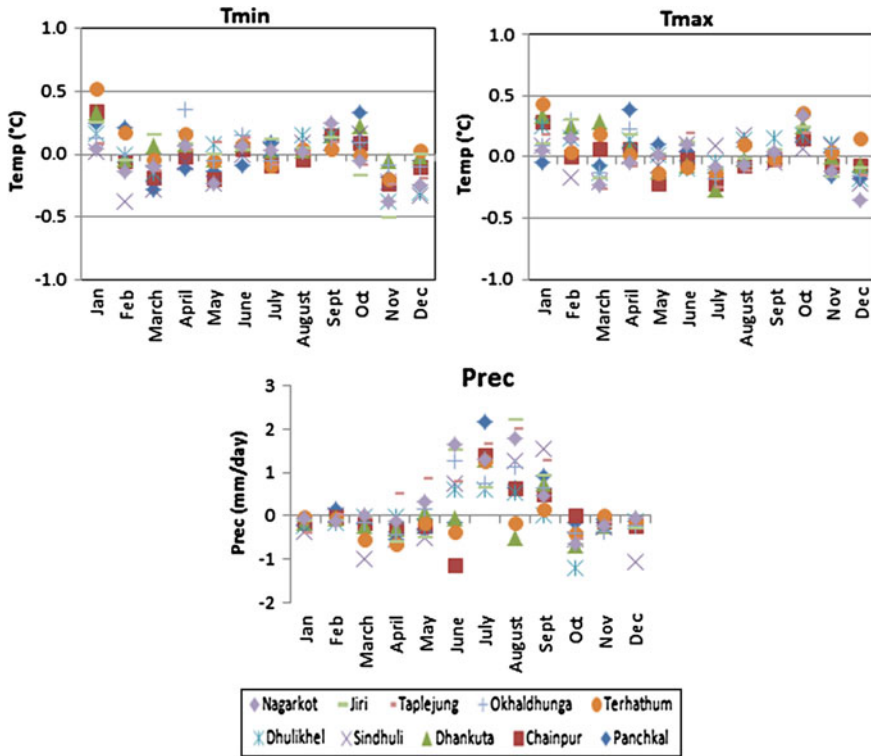


Fig. 2 Bias in mean monthly T_{min} (°C), T_{max} (°C), and precipitation between the observed and LARG-WG simulated data for the baseline period (1971–2000) for ten stations in the Koshi basin. The bias is calculated as observed minus simulated

bias. The results indicate that LARS-WG simulated temperature and precipitation agreed well with the observed values, and thus, the model can be used for down-scaling future climate data in this study.

3.1.2 SWAT

The SWAT model was calibrated using streamflow measured at the Saptakoshi outlet (Chatara) and its major tributaries (Arun, Tamor, and Sun Koshi) (Fig. 3). The available observed flow data were split for calibration (1990–2000) and validation (2001–2008) purposes. The most sensitive parameters were chosen in the calibration procedure based on literature review and a preliminary sensitivity analysis of the parameters. The sensitive parameters for the Koshi basin are presented in Table 2. The value of the sensitive parameters was adjusted within the appropriate ranges as defined in SWAT documentation to obtain the best calibration for the model. The calibration and validation results for the SWAT model are

Fig. 3 River network of the Koshi basin and calibration points considered in this study



presented in Table 3. The values of performance indicators R^2 , NS, and PVE were well under the acceptable limit of $R^2 > 0.60$, $NS > 0.50$, and $PVE < 15\%$ (recommended by Santhi et al. (2001) and Van Liew et al. (2007)) during calibration and validation periods. The PVE in Tamur was higher, as the flow in Tamur was under predicted during both calibration and validation periods. The hydrographs for observed and simulated flow of the Saptakoshi outlet (Chatara) is shown in Fig. 4. These results indicate that the model performance was satisfactory, and thus, it can be extended to study the effect of climate change on water balance and streamflow of the Koshi basin. The model parameters calibrated for the past periods are assumed to remain valid for the future period simulations. The land use in the Koshi basin is also assumed to remain unchanged in the future periods for this study.

Table 2 Parameters considered for the SWAT model calibration

Parameters	Description	Default value	Range
CN2	Curve number	38–91	35–98
ESCO	Soil evaporation compensation factor	0	0–1
SOL_AWC	Available water capacity of the soil layer (mm H_2O/mm soil)	0.21	0–1
RCHRG_DP	Deep aquifer percolation fraction	0.05	0–1
GW_REVAP	Groundwater “revap” coefficient	0.02	0.02–0.20
GW_Delay	Groundwater delay from soil to channel (days)	31	0–500
GWQMN	Threshold depth of water in the shallow aquifer required for return flow to occur (mm H_2O)	0	0–500
Alpha_bf	Baseflow alpha factor (days)	0.048	0–1
CH_K2	Channel effective hydraulic conductivity (mm/h)	0	0–500
SOL_K	Saturated hydraulic conductivity (mm/h)	51.6	0–2,000

Table 3 Calibration and validation statistics for the Koshi River Basin and its tributaries

	Calibration (1990–2000)			Validation (2001–2008)		
	R2	NS	PVE (%)	R2	NS	PVE (%)
Sun Koshi	0.84	0.82	3.3	0.85	0.83	-2
Arun	0.60	0.58	-12	0.61	0.51	0
Tamur	0.84	0.57	-39	0.88	0.66	-36.4
Saptakoshi	0.87	0.85	-12.3	0.84	0.83	-10.7

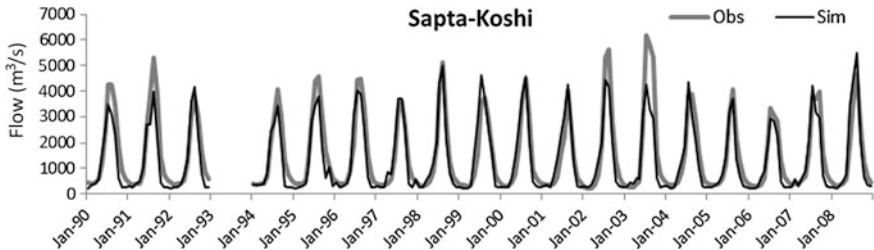


Fig. 4 Observed and simulated monthly streamflow at the Saptakoshi outlet during calibration and validation periods

3.2 Baseline Period Simulations

The performance of the SWAT model was analysed using the baseline period observed and simulated data. This analysis helps to check the consistency of weather data simulated using LARS-WG for its application to simulate the hydrological parameters of the Koshi basin. The annual water balance components of the Koshi basin using observed and simulated weather data are presented in Table 4. The annual surface runoff and baseflow were simulated with a difference of 0.2 and 1.5 %, respectively. The total water yield was simulated with a difference of less than 1 %. The difference between observed and simulated values of actual ET and potential ET is also less than 1 %. This indicates that the baseline period weather data simulated from LARS-WG performs well for the Koshi basin. This increases the confidence of using LARS-WG simulated climate data to analyse impacts of climate change on the water resources of the Koshi basin. The annual water balance of the Koshi basin suggests that the total water yield accounts for nearly 67 % of the total precipitation. The evapotranspiration and deep percolation represent 23 and 10 % of the annual precipitation. The monthly water balance of the Koshi basin presented in Table 5 indicates that the majority of precipitation (75 %), surface runoff (65 %), and water yield (76 %) are concentrated during the four months of the monsoon season (JJAS). Minimum flow is observed during the winter season (DJF), which is less than 5 % of the total annual flow.

Table 4 Annual average water balance components of the Koshi basin simulated using observed and LARS-WG simulate climate for the baseline period (1981–2000)

	Rain	Surf Q	Baseflow	WY	ET	PET
Simulated using observed climate	1,033.9	244.7	431.6	676.3	274.8	747.1
Simulated using LARS-WG simulated climate	1,041.9	243.1	425.5	668.6	276.7	754.2
Difference (%)	-0.8	0.7	1.4	1.1	-0.7	-1.0

Table 5 Monthly water balance components of the Koshi basin simulated using LARS-WG simulated climate for the baseline period (1981–2000)

	Precipitation (mm)	Surf Q (mm)	Water Yield (mm)	ET (mm)	PET (mm)
Jan	12.2	0.45	9.62	4.25	30.7
Feb	15.74	0.36	7.11	5.57	38.01
Mar	26.72	2.91	11.64	11.95	64.33
Apr	46.29	7.47	22.82	21.3	80.7
May	79.33	15.23	44.9	32.79	91.08
Jun	153.28	33.33	91.38	39.64	85.18
Jul	248.33	66.05	156.26	46.66	83.36
Aug	236.67	66.91	154.62	44.46	79.42
Sept	148.48	38.26	100.15	33.72	67.74
Oct	51.73	10.14	39.87	21.06	58.86
Nov	13.12	1.43	17.4	10.19	42.31
Dec	9.98	0.55	12.79	5.14	32.54

3.3 Climate Projections for Future Periods

The climate projections for three future periods (2020s, 2055s, and 2090s) relative to the baseline period (1981–2000) are presented in this section. The downscaled temperature and precipitation projections of 25 ensembles were used to analyse the range of projections for three future periods. The box-whisker plots are used to represent the uncertainty arising in projections from GCMs and the scenarios. The upper and lower boundaries of the boxes represent the 25th and 75th percentiles respectively, while the line in the box shows the median values. The ticks outside the boxes show the maximum and minimum value of the projected changes. The results are presented and discussed for changes in mean monthly values of climate variables (T_{\min} , T_{\max} , and precipitation) projected by ten GCMs under the A1B scenario, and in annual values projected by all GCMs under the three scenarios.

3.3.1 Temperature

The change in mean monthly temperature projected by ten GCMs under the A1B scenario, relative to the baseline period, is shown in Fig. 5. The change in annual temperature, as projected by the GCMs under the three scenarios: B1, A1B, and A2 for three future periods (relative to the baseline period), is shown in Fig. 6. Projections of all the GCMs under the A1B scenario (Fig. 5) indicate an increase in both T_{min} and T_{max} in each month for all three future periods. While the GCMs do not agree on the magnitude of change, they do project that the range of temperature change within each month will increase with the time horizon. The projections of annual T_{min} and T_{max} during the 2020s, as shown in Fig. 6, are within the narrow range of 0.5–1.5 °C with almost similar median values. This indicates that T_{min} and T_{max} projections during the 2020s are expected to be similar, irrespective of the scenario that may follow. The differences between projected values of T_{min} and T_{max} become greater in accordance with the choice of the scenario during the mid-century and the late-century periods. This heightened difference is because of the significant increase in differences among the different emission scenarios themselves. The differences among the median values of projections justify this finding: during the 2090s for T_{max} , the median value as projected under the A2 scenario is 1.6 °C higher than as projected under the B1 scenario. This may influence runoff in the basin and monthly water availability especially during the dry season.

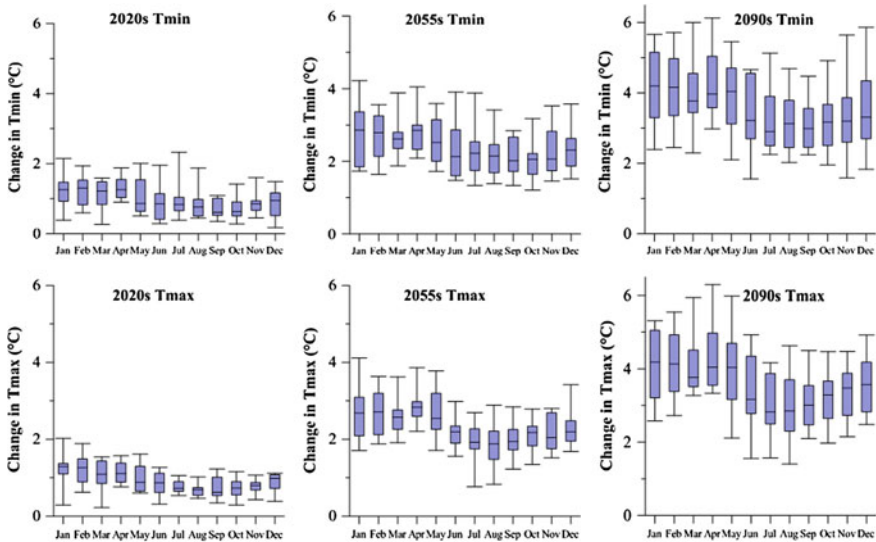


Fig. 5 Changes in average monthly T_{min} and T_{max} under the A1B scenario for the 2020s, 2055s, and 2090s relative to the baseline period

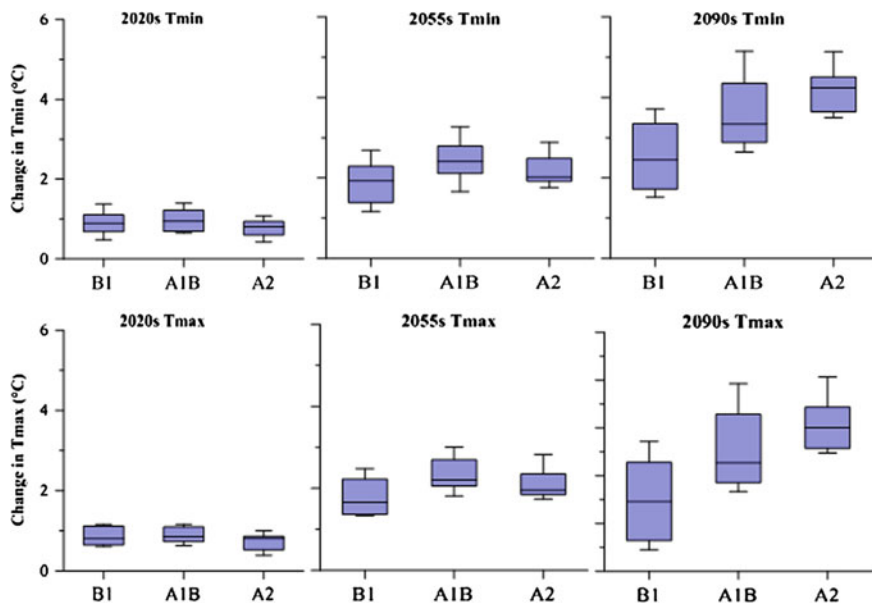


Fig. 6 Changes in annual average T_{\min} and T_{\max} for the 2020s, 2055s, and 2090s relative to the baseline period

3.3.2 Precipitation

The relative changes in mean monthly precipitation for the three future periods relative to the baseline period, as projected by the ten GCMs under the A1B scenario, are shown in Fig. 7. The changes in annual precipitation, as projected by the GCMs for all three scenarios (B1, A1B, and A2), are shown in Fig. 8. From Figs. 7 and 8, it can be gleaned that there is a wide variation among the GCMs regarding the projected change in precipitation. The range of projected change in monthly and annual precipitation increases with an increase in the time horizon. The changes in precipitation are not univocal and range from negative to positive for all three future periods. Figure 7 indicates that no clear pattern in the precipitation change is evident in any month. This may be due to the complexity that arises when interpreting precipitation projections, since different GCMs often do not agree on whether precipitation will increase or decrease at a specific location; they agree even less on the magnitude of that change (Girvetz et al. 2009). A higher difference is projected during the four months of the summer season (JJAS), perhaps because more than 70 % of the total annual rainfall is concentrated during this time. The relative change for all the months is almost similar to what is shown in Fig. 7, but the absolute change in the eight months of the non-monsoon period (October to May) is very small compared to the change in the monsoon period itself (June to September). The median values in Fig. 7 also indicate that a positive change is more

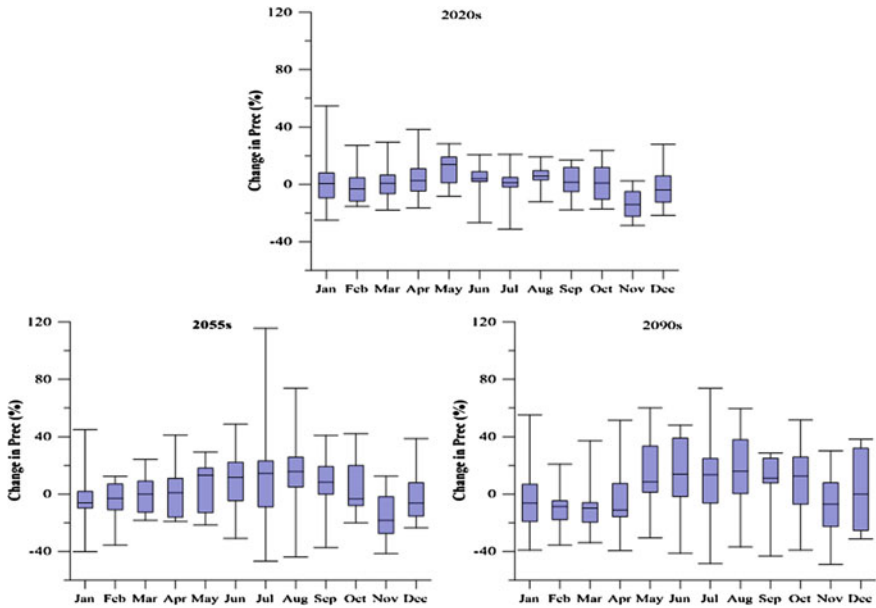


Fig. 7 Changes in average monthly precipitation under the A1B scenario for the 2020s, 2055s, and 2090s relative to the baseline period

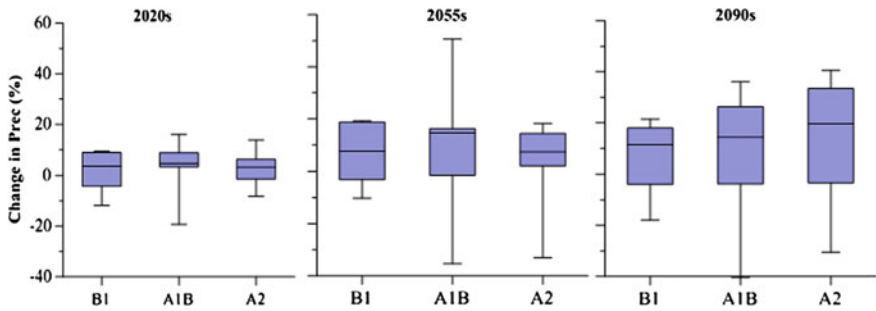


Fig. 8 Changes in annual precipitation for the 2020s, 2055s, and 2090s relative to the baseline period

likely in the summer season while a negative change is more likely in the winter season (DJF). The changes in annual precipitation, as projected under the three scenarios (Fig. 8), also indicate that the difference in projections increase with the time horizon. The median value indicates a positive change in annual precipitation under all three scenarios. Also, the median value for the three scenarios is closer to each other during the early-century period but shows significant differences during the mid- and late-century periods. It is important to note here that the scenario uncertainty is estimated based on three IPCC SRES scenarios, and with the

development of new RCP scenarios, the estimates could be improved. For longer lead-time predictions, assessments of the relative importance of model and uncertainty scenarios may change as a result of including new processes in climate models (e.g. better representation of biogeochemical and ice-sheet feedbacks) and improved understanding of scenarios (Hawkins and Sutton 2010).

3.4 Impacts on Hydrology and Water Balance Components

The calibrated and validated SWAT model was used to analyse the impacts of climate change in three future periods of the 2020s, 2055s, and 2090s. The future climate data from all 25 ensembles were used to analyse the range of projections of hydrological and water balance components. The change in hydrological parameters and water balance components in future periods relative to the baseline period (1981–2000) is presented and discussed here.

3.4.1 Mean Monthly Flow

The flow during the baseline period and the change (in percentage) in the flow during the three future periods are presented in Table 6. The values in Table 6 represent the mean value of change from all GCMs under the respective scenarios. It has been found that the flow increases in all the months during all three future periods, except for June and November in the 2020s, where the flow slightly decreases (less than 1 %). The increase in flow is higher during the summer season (June to September). This indicates that the change in flow is directly related to the change in precipitation. The highest increase in flow is projected during the month of August, and subsequently, the peak flow is expected to shift from the month of July to August under all three scenarios. The maximum increase (of 48 %) is projected under the A2 scenario in August during the 2090s. During the autumn season, the change in flow is not significant in the 2020s, but a high increase is projected in the 2055s and 2090s especially for the month of October. The flow is also projected to increase during all three months of the winter season. The maximum increase of flow (9 %) is projected during the winter season months under the A2 scenario during the 2090s. The spring season flow shows a significant increase during all three future periods. This increase might be due to the increase in temperature, which in turn may cause early snow melt.

3.4.2 Changes in Seasonal and Annual Flow

The changes in seasonal and annual flows, as projected by ten GCMs under the A1B scenario, for all three future periods (with respect to the baseline period's seasonal and annual flow), are shown in Fig. 9. The solid blue bar in this figure

Table 6 Mean monthly flow at Chatara during the baseline period and changes in the flow (in percentage) during the three future periods

	Baseline (m ³ /s)	2020s			2055s			2090s		
		B1	A1B	A2	B1	A1B	A2	B1	A1B	A2
		% change with respect to baseline								
Jan	380.6	3.3	3.3	4.9	6.2	6.0	4.3	5.1	7.5	8.9
Feb	340.5	3.3	3.6	5.1	4.7	5.6	3.8	6.9	6.7	8.7
Mar	364.5	1.8	4.1	3.5	4.6	8.0	4.4	5.5	8.3	12.2
Apr	524.1	5.9	12.3	7.7	8.5	14.2	11.1	12.6	14.1	16.8
May	928.4	8.3	14.4	3.1	9.3	12.4	13.0	9.9	20.1	12.1
Jun	2,002.2	2.9	6.9	-0.9	6.8	17.4	6.7	7.4	20.9	14.4
Jul	3,286.8	4.2	5.1	8.4	12.3	26.3	6.6	16.5	25.3	34.9
Aug	3,249.3	9.8	10.5	13.6	25.6	27.7	12.0	25.6	29.7	48.4
Sep	2,307.6	0.7	4.8	3.0	12.0	17.1	3.9	11.8	20.9	33.0
Oct	1,001.8	1.7	4.0	1.5	10.3	12.2	4.4	11.2	19.6	27.4
Nov	546.2	0.3	-0.9	-1.0	4.2	3.2	0.9	2.9	6.6	11.5
Dec	441.4	3.2	1.5	3.3	6.2	5.3	5.0	4.1	6.7	9.0

represents the mean of the ten GCMs under the A1B scenario. The results indicate that there are likely chances of an increase in seasonal as well as annual runoff in all three future periods as the majority of GCMs and their mean indicates. Among the ten GCMs considered here, only two CSMK and IPCM indicate a decrease in flow. The maximum relative increase (of 12 %) is projected for spring during the 2020s, while increases of 23 and 25 % are projected, respectively, for the summers of the 2055s and 2090s. The range of change in seasonal and annual flow (not shown here) varies from negative to positive under all three scenarios. The uncertainty in projection increases with the increase in time periods with much higher differences during the 2090s compared to the 2020s.

3.4.3 Water Yield

The changes in monthly and annual water yield for the three future periods relative to the baseline period are shown in Figs. 10 and 11. Both monthly and annual water yield during the early-century period (2020s) are expected to change by only a small amount as median values indicate. The middle 50 % range (box in Figs. 10 and 11) indicates that the differences in the GCMs' projections are within the narrow range, with a maximum difference projected for April during the 2020s. The difference in projections of water yield increases with the time horizons. The median value indicates a positive change during the 2055s and 2090s with the exception of April and May in the 2090s. A smaller difference between the median values and narrow range of projections in Fig. 11 also indicates that the relative annual change is dominantly affected by GCMs rather than by SRES scenarios

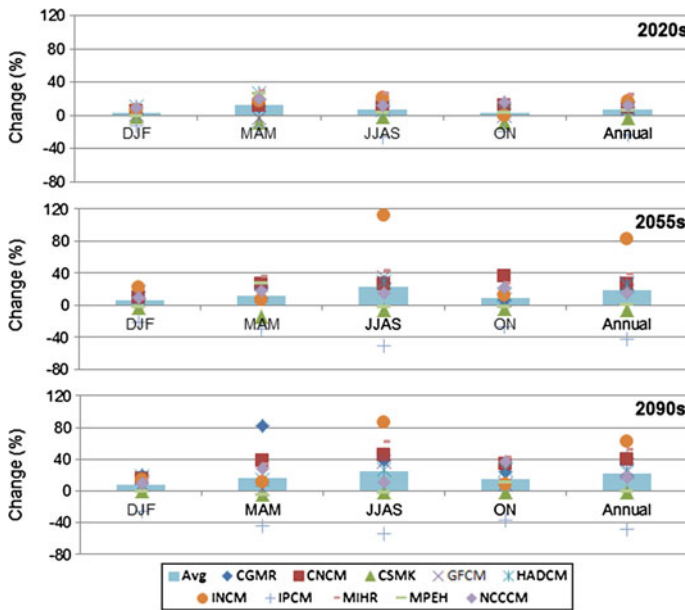


Fig. 9 Projected changes in seasonal and annual runoff at the Saptakoshi outlet according to ten GCMs under the A1B scenario for three future periods relative to the baseline period. The blue solid bar represents the mean of ten GCMs

during the 2020s. During the 2055s, both scenarios and GCMs are affected by the change in water yield. The median value indicates an increase during the 2055s under all three scenarios with the highest increase under the A1B scenario. The projections for precipitation as shown in Figs. 7 and 8 also indicate a higher chance of increase during the 2055s. During the 2090s, both GCMs and scenarios show a dominant effect on the water yield in the basin, with a more likely chance of increase.

3.4.4 Potential ET

The relative changes in potential ET for three future periods with respect to the baseline period are shown in Fig. 12. The PET value is projected to increase during all three future periods according to all the GCMs, with the exception of INCM during the monsoon season. INCM indicates a decrease in PET which might be because of its temperature projections which show the least increase during the monsoon season among all the GCMs under the A1B scenario. Temperature increase, as projected by all the GCMs, is the main factor causing an increase in PET. The average monthly PET varies significantly with the change in temperature. Results indicate that the increase in PET is highest in the months of the winter season (DJF) which are also expected to show a maximum increase in temperature,

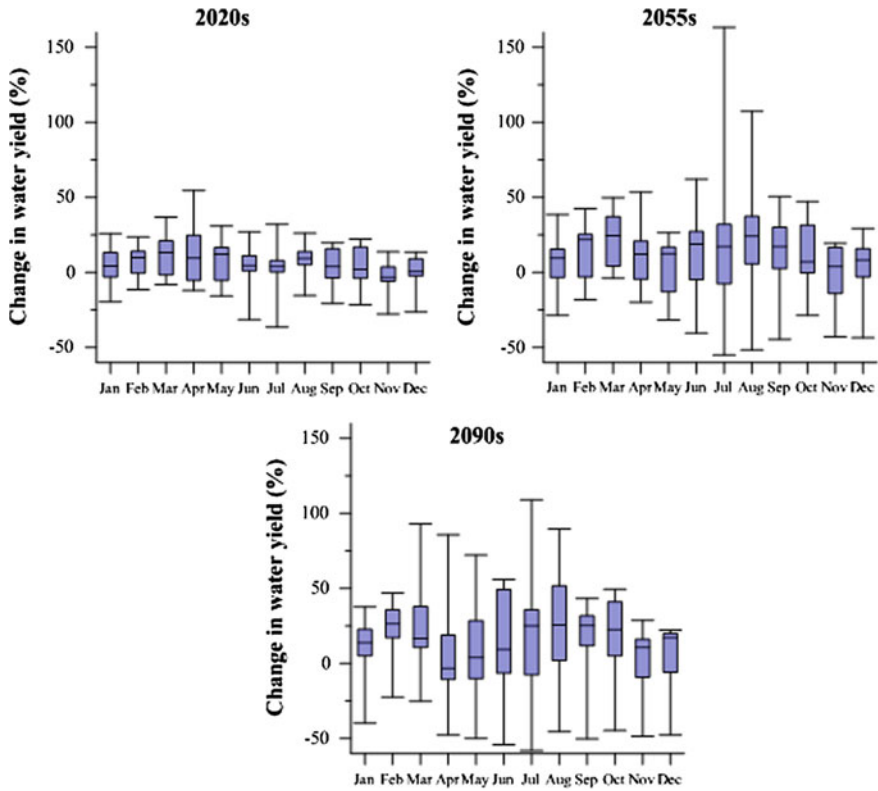


Fig. 10 Changes in average monthly water yield under the A1B scenario for the 2020s, 2055s, and 2090s relative to the baseline period

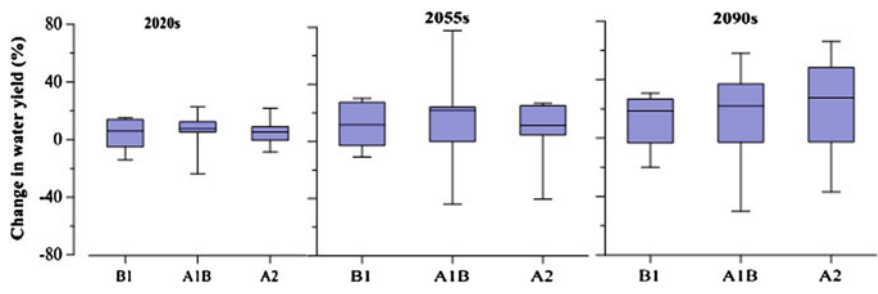


Fig. 11 Changes in annual average water yield for the 2020s, 2055s, and 2090s relative to the baseline period

while the minimum increase is projected for the summer season (JJAS) during all three future periods. The relative change in average annual PET (Fig. 13) also indicates an increase during all three future periods. All GCMs under three

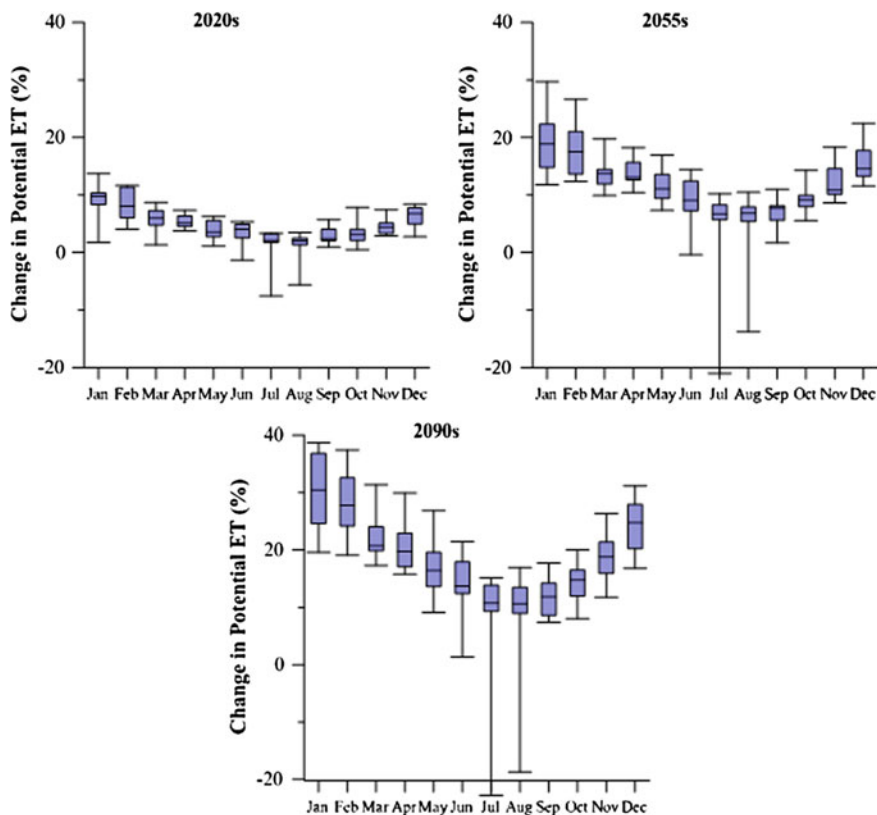


Fig. 12 Changes in average monthly potential ET under the A1B scenario for the 2020s, 2055s, and 2090s relative to the baseline period

scenarios indicate an increase in PET value although uncertainty exists as to the magnitude of change. During the 2020s, uncertainty in the projected change in PET varies in the narrow range from 1.7 to 5.5 % compared to the value of baseline period. The range of projections increases with the time horizons: 4.2–13.7 % in the 2055s and 6.8–24 % in the 2090s.

3.4.5 Actual ET

The relative change in mean monthly and annual value of actual ET is more likely to increase during all the three future periods, as middle 50 % values indicate in Figs. 14 and 15. Two GCMs (INCM and IPCM) indicate a decrease in ET values in certain months, especially during the summer's season. An analysis of the change in temperature and precipitation shows INCM's projected minimum increase in temperature and IPCM's projected maximum decrease in precipitation among the ten GCMs

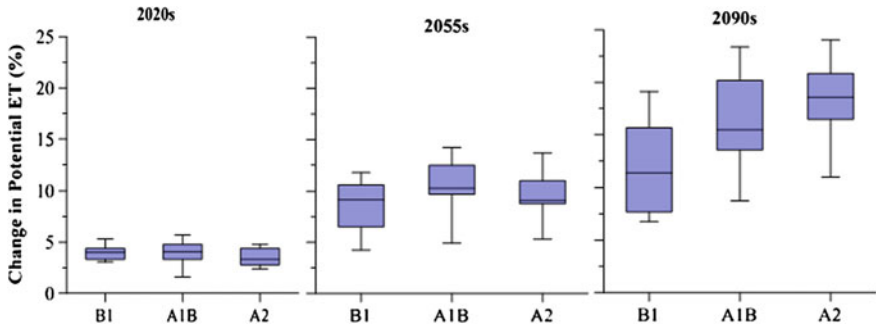


Fig. 13 Changes in annual average potential ET for the 2020s, 2055s, and 2090s relative to the baseline period

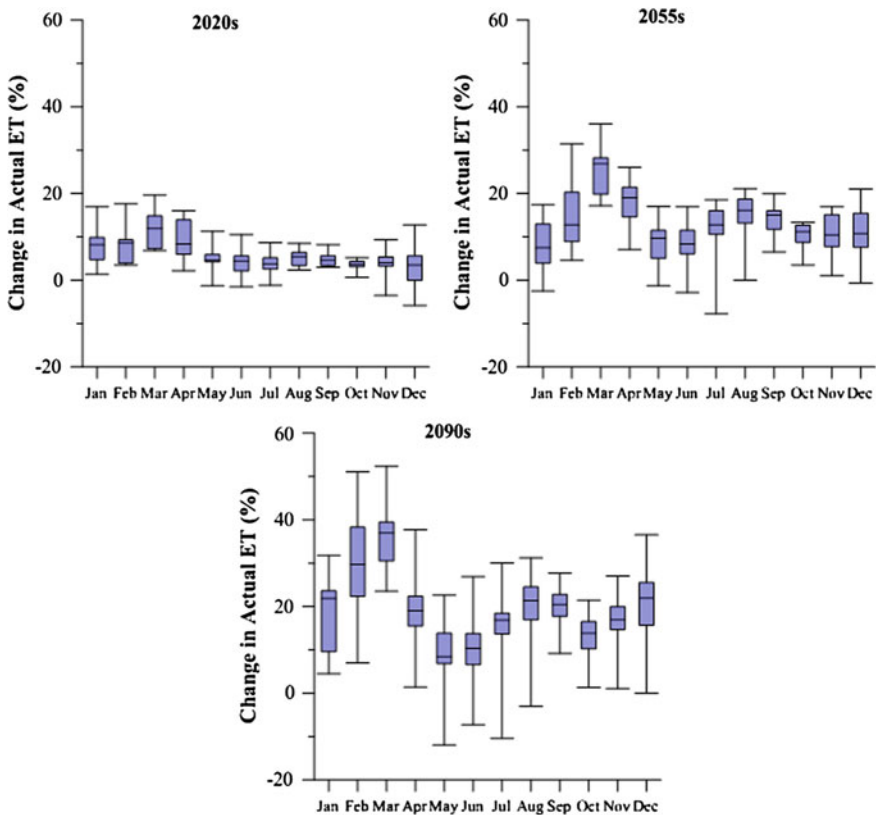


Fig. 14 Changes in average monthly actual ET under the A1B scenario for the 2020s, 2055s, and 2090s relative to the baseline period

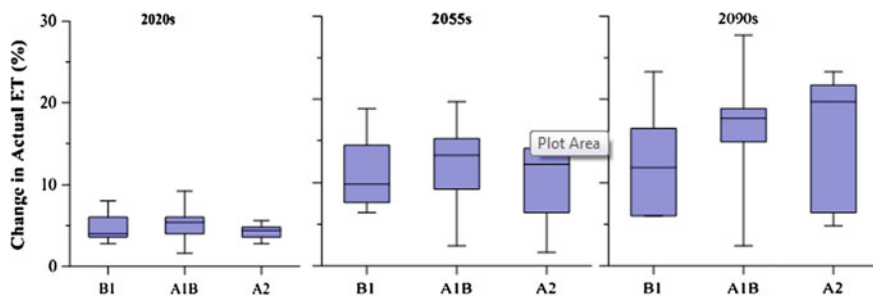


Fig. 15 Changes in annual average actual ET for the 2020s, 2055s, and 2090s relative to the baseline period

under the A1B scenario. The highest relative change in ET is projected during the months of February, March, and April. The increase in ET is also higher during winter than summer. The projections from all GCMs under three scenarios (B1, A1B, and A2) indicate an increase in annual ET during all three future periods. The median value of change in ET indicates maximum increase under the A1B scenario during the 2020s and 2055s and under the A2 scenario during the 2090s.

4 Conclusions

This study used a multi-model, multi-scenario approach to analyse the impacts of climate change on the hydrology of the Koshi River Basin. Three SRES scenarios (B1, A1B and A2) assuming a distinctly different direction for future development were selected for this study. Multiple GCM projections for each of the three scenarios were used. A statistical downscaling model (LARS-WG) was selected to downscale the global scale projections to the basin scale. The physically based hydrological model Soil and Water Assessment Tool (SWAT) was used to analyse the impacts of climate change on hydrology.

LARS-WG-simulated climate data for the baseline period (1971–2000) showed good performance with the historical climate of the Koshi basin. Calibration and validation results of the SWAT model suggest that it can be applied with confidence in this study. The results indicate that the Koshi basin will tend to become warmer in the future as projected by all GCMs under three SRES scenarios. Annual average T_{\max} will rise by 2.6, 3.6, and 4.2 °C in the 2090s as per B1, A1B, and A2 scenarios, respectively, considering the mean of all GCMs under each of the scenarios. The projected change in precipitation is not uni-directional which might increase or decrease in future periods. The majority of the GCMs (8 out of 10) considered here and the mean value of projections from all GCMs under each of the three scenarios indicated an increase in future precipitation. The maximum difference in precipitation projections is simulated under the A1B scenario with a range

varying from 38 to 50 % in the 2055s. A large uncertainty range exists in the projections of flow with results indicating both decrease and increase for all three future periods. The mean monthly and annual flow is expected to increase as projections from the majority of GCMs and the mean value of all GCMs indicates. The maximum increase in flow is projected during the spring season with increases of 23 and 25 % during the 2055s and 2090s, respectively, under the A1B scenario. This high increase in spring flow indicates the need for more flood control measures in the Koshi basin. The water balance components: surface flow, baseflow, and water yield may decrease or increase in future periods, as GCMs do not agree on the direction of change. The potential ET and actual ET are projected to increase as projections from all GCMs and scenarios indicate, although major uncertainty exists as to the magnitude of change. The potential ET is projected to increase in the range of 6–24 % in the 2090s.

There is high variability among the models and scenarios for projections, and the variability increases with future time periods. Although inter-model variability exists in each of the scenarios, for the early-century period, the differences among the scenarios are much less. During the mid- and late-century periods, inter-model variability in all climatic and hydrological variables increases, resulting in higher projection uncertainty. The multi-model and multi-scenario approach presented in this paper helps in understanding the uncertainty linked to future climate projections and the impact on water resources. Although different downscaling techniques and hydrological model parameters also bring uncertainty in projections, it is expected that the large variability induced by different GCMs and GHG emission scenarios, as shown in this paper, will dwarf those induced by other sources. The impacts of climate change on the hydrology and water resources of the Koshi basin will further affect all water use sectors which may be analysed considering the findings from this study.

Acknowledgment This study was funded in part through the UNESCO-IHE Partnership Research Fund (UPaRF) under the AGloCAP (Adaptation to Global Changes in Agricultural Practices) project and in part through the Asian Institute of Technology (AIT) research fellowship. The authors would like to thank the Department of Hydrology and Meteorology (DHM), Nepal for the meteorological data used in this study, which was made available for the AGloCAP project.

References

- Agrawala S, Raksakulthai V, Aalst MV, Larsen P, Smith J, Reynolds J (2003) Development and climate change in nepal: focus on water resources and hydropower. Organisation for Economic Co-operation and Development (OECD). <http://www.oecd.org/dataoecd/6/51/19742202.pdf>
- Anandhi A, Srinivas VV, Nanjundiah RS, Kumar DN (2008) Downscaling precipitation to river basin in India for IPCC SRES scenarios using support vector machine. *Int J Climatol* 28:401–420
- Bartlett R, Bharati L, Pant D, Hosterman H, McCornick P (2010) Climate change Impacts and adaptation in Nepal. Colombo, Sri Lanka: International Water Management Institute. 35p. (IWMI Working Paper 139). doi:10.5337/2010.227

- Bastola S, Murphy C, Sweeney J (2011) Role of hydrological model uncertainty in climate change impact studies. *Adv Water Resour* 34(5):562–576
- Chhetri MBP (2010) Effects of climate change: the global concern. In: Proceedings of the 4th AMCDRR 25-28 October 2010 Republic of Korea. <http://www.iawe.org/WRDRR/2010/Meena.pdf>
- Chiew FHS, Kirono DGC, Kent DM, Frost AJ, Charles SP, Timbal B, Nguyen KC, Fu G (2010) Comparison of runoff modeled using rainfall from different downscaling methods for historical and future climates. *J Hydrol* 387:10–23
- Dibike YB, Coulibaly P (2005) Hydrologic impact of climate change in the Saguenay watershed: comparison of downscaling methods and hydrologic models. *J Hydrol* 307:145–163
- Ficklin DL, Luo Y, Luedeling E, Zhang M (2009) Climate change sensitivity assessment of a highly agricultural watershed using SWAT. *J. Hydrology* 374:16–29
- Girvetz EH, Zganjar C, Raber GT, Maurer EP, Kareiva P et al (2009) Applied climate-change analysis: the climate wizard tool. *PLoS ONE* 4(12):e8320. doi:10.1371/journal.pone.0008320
- Hawkins E, Sutton R (2010) The potential to narrow uncertainty in projections of regional precipitation change. *Clim Dyn* 37:407–418
- IPCC (2007) *Climate Change 2007: the physical science basis*. In: Solomon S, Qin D, Manning M, Chen Z, Marquis M, Averyt KB, Tignor M, Miller HL (eds) *Contribution of WG I to AR4 of IPCC*. Cambridge University Press, ISBN 978-0-521-88009-1 (pb: 978-0-521-70596-7)
- Maraun D, et al (2010) Precipitation downscaling under climate change. Recent developments to bridge the gap between dynamical models and the end user. *Rev Geophys* doi:10.1029/2009RG000314
- Minville M, Brissette F, Leconte R (2008) Uncertainty of the impact of climate change on the hydrology of a nordic watershed. *J Hydrol* 358:70–83
- Moriondo M, Bindi M (2006) Comparison of temperatures simulated by GCMs, RCMs And statistical downscaling: potential application in studies of future crop development. *Clim Res* 30:149–160
- Nguyen VTV (2005) Downscaling methods for evaluating the impacts of climate change and variability on hydrological regime at basin scale. *Role of water sciences in transboundary river basin management, Thailand*
- Santhi C, Arnold JG, Willams JR, Dugas WA, Srinivasan R, Hauck LM (2001) Validation of the SWAT model on a large river basin with point and nonpoint sources. *J Am Water Resour Assoc (JAWRA)* 37(5):1169–1188
- Semenov MA, Barrow EM (1997) Use of stochastic weather generator in the development of climate change scenarios. *Clim Change* 35:397–414
- Semenov MA, Stratonovitch P (2010) The use of multi-model ensembles from global climate models for impact assessments of climate change. *Clim Res* 41:1–14
- Sharma E, Bhuchari S, Xing M, Kothyari BP (2007) Land use change and its impact on hydro-ecological linkages in Himalayan watersheds. *Tropical Ecol* 48(2):151–161
- Shrestha AB, Devkota LP (2010) *Climate change in the Eastern Himalayas: Observed trends and model projections. Climate change impact and vulnerability in the Eastern Himalayas-Technical report 1*. ICIMOD, Kathmandu
- Stott PA, Kettleborough JA (2002) Origins and estimates of uncertainty in predictions of twenty first century temperature rise. *Nature* 416:723–726
- Tisseuil C, Vrac M, Lek S, Wade AJ (2010) Statistical downscaling of river flows. *J Hydrol* 385:279–291
- Van Liew MW, Veith TL, Bosch DD, Arnold JG (2007) Suitability of SWAT for the conservation effects assessment project: a comparison on USDA-ARS experimental watersheds. *J. Hydrol Eng* 12(2):173–189
- WWF (2009) *Climate change impact on discharge at Koshi River Basin using regional climate and hydrological models. Final report on a collaborative project of WWF-Nepal/DHM*
- Zhang H, Huang GH, Wang D, Zhang X (2011) Uncertainty assessment of climate change impacts on the hydrology of small prairie wetlands. *J Hydrol* 396:94–103